March 28, 2017 Volume 33, Number 12 pubs.acs.org/Langmuir

LANGMUIR

The ACS journal of fundamental interface science

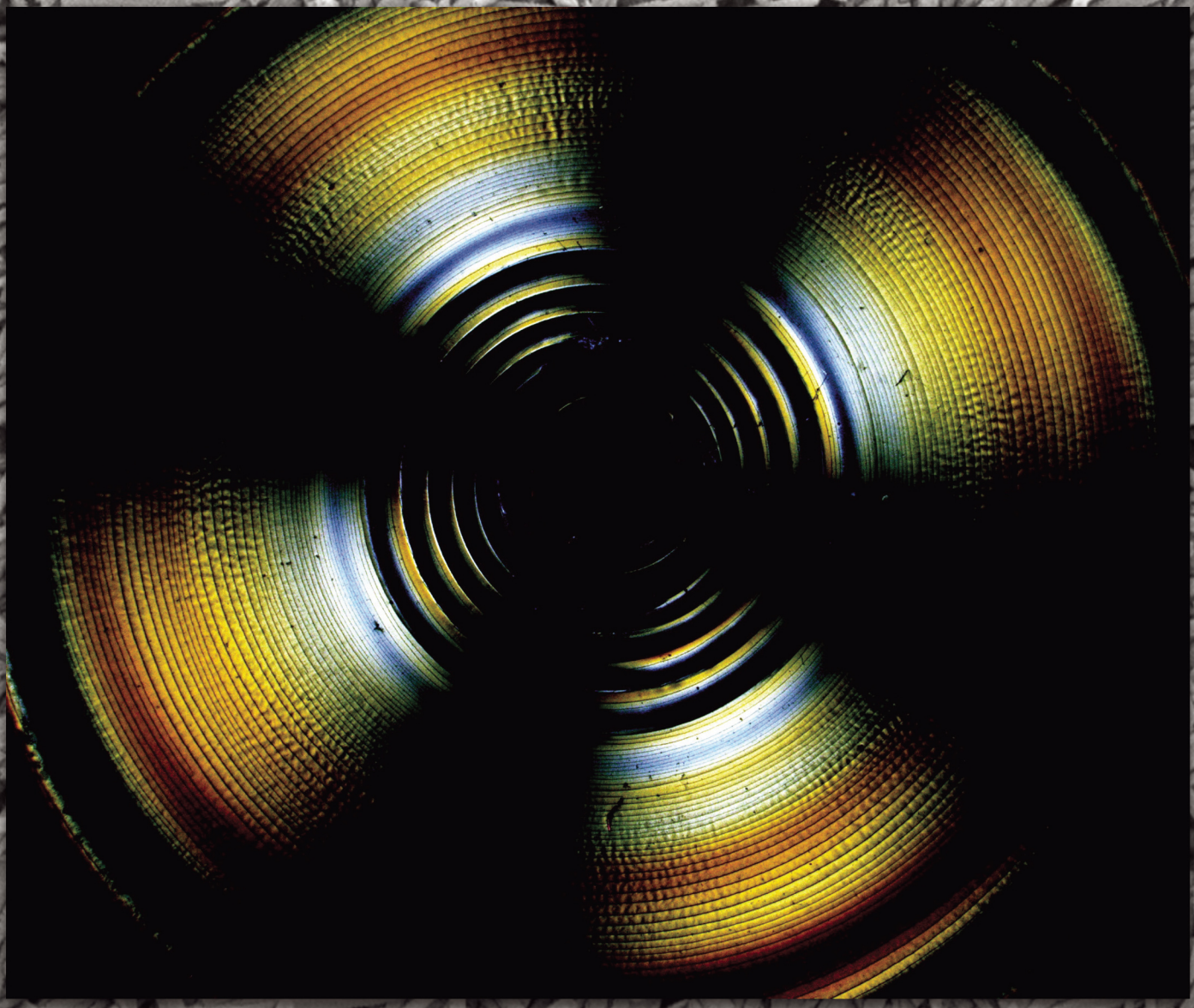

Self-Assembling Halloysite Nanotubes into Concentric Rings with a Maltese Cross-like Pattern

ACS Publications
Most Trusted. Most Cited. Most Read.

www.acs.org

LANGMUIR

Article

pubs.acs.org/Langmuir

Self-Assembling Halloysite Nanotubes into Concentric Ring Patterns in a Sphere-on-Flat Geometry

Mingxian Liu,* Zhuohao Huo, Tengfei Liu, Yan Shen, Rui He, and Changren Zhou*

Department of Materials Science and Engineering, Jinan University, Guangzhou 510632, PR China

Supporting Information

ABSTRACT: Highly ordered and concentric ring patterns consisting of halloysite nanotubes (HNTs) with hierarchical cholesteric architectures are prepared by evaporation-induced self-assembly in a sphere-on-flat geometry. The structure and properties of HNTs are investigated. HNTs show a perfect tubular morphology on the nanoscale with high dispersion stability in water. Upon drying the HNTs aqueous suspension in a sphere-on-flat confined space, regular concentric HNTs rings are formed on the substrate via a self-assembly process. The widths of the inner and outer rings and the spacing between the adjacent rings increase with an increase in the concentration of the HNTs suspension. The highly ordered and concentric HNTs rings show a pronounced Maltese cross-like pattern under crossed polarizers, which suggests the formation of hierarchical cholesteric architectures. Scanning electron microscopy and atomic force microscopy observations show a disclination alignment of HNTs in the ring strips, especially with a high concentration of the HNTs suspension. The patterned rough surfaces of the HNTs show low cytotoxicity and can be used as a cell-supporting scaffold. The HNTs rings can guide the growth and orientation of C2C12 myoblast cells perpendicular to the rings. This work provides a simple, repeatable, mild, and high-efficiency method for obtaining HNTs with hierarchical architectures, which show potential for a large variety of applications, for example, in vascular grafts and skin regeneration.

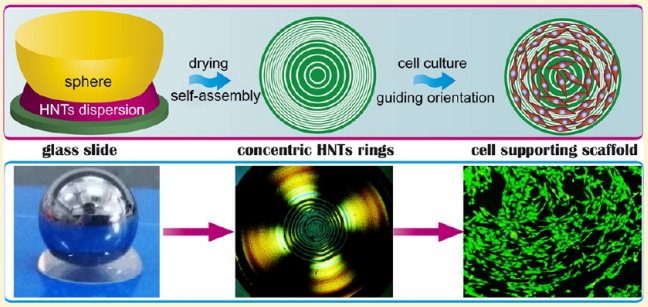

1. INTRODUCTION

There are many examples in nature of large-scale complex hierarchical architectures composed of nanosized inorganics and organic polymers, that is, nacre and bone.[1] The highly regular brick-and-mortar arrangement of inorganic and organic elements leads to composite materials with distinctive mechanical properties and multiple functionalities. Researchers have learned how to design artificial hierarchical architectures with ultrahigh mechanical properties and unique biofunctionalities from natural assembly processes.

However, to explore proper nanoparticles for self-assembly and precisely control the assembly behavior is fundamentally essential not only to elucidate the principles that underlie the evolution of complex hierarchical structures in nature but also to inspire the development of novel materials where their functionalities are encoded in the building blocks that compose them.[2] Anisotropic nanoparticles with a high aspect ratio should self-assemble into liquid−crystalline phases[3,4] in aqueous media, which can be further transferred into macroscopic ordered materials via evaporation of the solvent.[5]

Rodlike virus,[6,7] gold nanorods,[8,9] halloysite nanotubes (HNTs),[10,11] semiconducting nanowires,[12] graphene nanoplates,[13] cellulose nanocrystals (CNCs),[2] proteins,[14] and so forth have been used to study the assembly behavior of highly regular architectures. In these studies, the capillary assembly method was used to achieve selective delivery of individual nanoparticles into suitable target sites on large-area substrates. The capillary assembly of nanoparticles technique is ideal for the precise definition of topographic features arbitrarily distributed over large surfaces, and it is also energy-efficient, time-saving, and cost-effective.[9] For example, rodlike tobacco mosaic virus (with aspect ratio 17) can assemble into ordered hierarchical structures in a glass capillary tube.[6] Hierarchical cholesteric architectures of CNCs can be obtained by the self-assembly of their aqueous droplets in a confined spherical geometry.[2] Solvent evaporation of a drop-induced self-assembly is recognized as a nonlithography route for the one-step creation of complex, large-scale hierarchical structures. Lin and co-workers prepared a series of hierarchical architectures via drying nanoparticle suspensions in confined spaces.[15] The capillary force at the contact line during the drying process of nanoparticle suspensions leads to a periodic pinning and depinning deposition process (i.e., "stick−slip" motion), which is responsible for the formation of regular hierarchical structures.

Naturally occurring HNTs, $Al_2Si_2O_5(OH)_4{\cdot}nH_2O$, are novel inorganic nanostructures used for constructing high-performance composites and biomaterials.[10,16−21] HNTs always show a perfect tubular morphology with an empty lumen structure. The diameter and length of HNTs range from 15 to 50 nm and

Received: December 12, 2016
Revised: December 23, 2016
Published: December 27, 2016

DOI: 10.1021/acs.langmuir.6b04460
Langmuir 2017, 33, 3088−3098

300 to 1500 nm, respectively, which gives an aspect ratio of 6−100. The outer surface of the HNTs is negatively charged with a zeta potential of approximately −25 mV, which makes them easily achieve a monodisperse state in an aqueous suspension. When the concentration of the HNTs suspension is beyond 25 wt %, the liquid-crystal phenomenon can be identified by the tubes arrangement.[22] Self-assembly of HNTs can also be performed in ionic liquids (ILs), which represent a technology for fabricating ionogel electrolytes with faster ion transport and larger anisotropic conductivity.[23] Our previous study also revealed that HNTs can be assembled into a highly ordered strip pattern surface in a glass capillary tube via drying the aqueous suspension of HNTs.[10] However, the colloidal stability of HNTs in water is critical for the self-assembly process. The stability of HNTs in water can be improved by adding polymers such as amylose, DNA, and pectin and surfactants such as sodium dodecanoate and decyltrimethylammonium bromide.[24−26] The self-assembly of such nanotubes offers a large variety of applications, for example, in high-performance composites, cell isolation interface, and electrochemical devices. Compared with other anisotropic nanoparticles, HNTs have the comprehensive advantages of high dispersion ability in water without chemical modification, unique empty tubular structure for loading drugs, and good biocompatibility, and they are abundant in nature at a low price.[27,28] Consequently, HNTs show promising applications in biomedical areas such as tissue engineering scaffolds, drug delivery vehicles, wound healing dressings, cell capture devices, and biosensors.[16,19−21]

Directing cell orientation and differentiation using aligned material scaffolds is a hot topic for the purpose of tissue engineering.[29,30] Aligned polymer fibers or high-aspect-ratio nanoparticles can induce the orientation growth of osteoblast, fibroblast, and myoblast cells.[6,8,31] The straightforward solutions for preparing micro- and nanoscale patterned substrates for guiding cell orientation both in vitro and in vivo are electrospinning and soft lithography. However, the electrospinning technique is less preferred because of disadvantages that include the use of organic solvents and the limited control of pore structures.[32] Polydimethylsiloxane (PDMS) microchannels fabricated using soft lithography techniques can regulate the aspect ratio, actin alignment, and phenotype switch of adherent vascular smooth muscle cells.[30,33] However, soft lithography depends on the use of hydrophobic and soft PDMS, which is easily distorted during application.[34]

Here, we report a simple, repeatable, mild, and high-efficiency approach for obtaining HNTs with hierarchical architectures on a large scale. Highly ordered and concentric ring patterns consisting of HNTs with hierarchical cholesteric architectures are prepared by evaporation-induced self-assembly in a sphere-on-flat geometry. The influence of the concentration of the HNTs suspension on the formation of the ringlike pattern was studied. The macroscopic liquid crystal with Maltese cross was correlated with the nanotube alignment in the rings. The HNTs rings were further used to regulate the C2C12 myoblasts behavior. This hierarchical cholesteric architecture of HNTs shows potential applications in tissue engineering, sensing, electronics, and optical fields.

2. EXPERIMENTAL SECTION

2.1. Materials. High-purity HNTs were purchased from Guangzhou Runwo Materials Technology Co., Ltd, China. 3-Aminopropyltriethoxy silane (APTES) and other chemicals were bought from Sigma-Aldrich. Ultrapure water from a Milli-Q water system (resistivity > 18 MΩ·cm^{-1}) was used to prepare the aqueous dispersion.

2.2. Preparation of HNTs Suspension. Purified HNTs were produced by centrifuging a 5 wt % raw HNTs aqueous suspension at 5000 rpm for 30 min.[35] Afterward, the supernatant was collected and concentrated at 80 °C under mechanical stirring to fixed concentrations of 0.5, 1, 2, and 4 wt %. The HNTs aqueous suspensions with different concentrations were very stable at room temperature and during the self-assembly process.

2.3. Formation of HNTs Rings in a Sphere-on-Flat Geometry. The sphere-on-flat geometry was constructed according to refs 36−39. HNTs aqueous suspension (200 μL) was loaded in a small gap between a silica sphere (diameter 12 mm, or stainless steel sphere) and a round glass sheet (cover glasses 801007, Nest Biotechnology Co., Ltd., diameter 15 mm and thickness 0.16 mm). The sphere and the glass sheet were firmly fixed at the top and bottom using a sample holder inside of a sealed chamber. The temperature of the chamber was 60 °C. The two surfaces (sphere and glass sheet) were brought into contact, thus forming a capillary bridge of the solution (Figure 2A). In such a sphere-on-flat geometry, evaporation occurred only at the capillary edge. Approximately 4 h was needed for the water evaporation to be completed. Finally, the two surfaces were separated and the patterns on the glass sheet were examined. If the suspension was dried at room temperature, the drying time was too long (several days). At a high drying temperature such as 90 °C, some bubbles could be found on the HNTs coatings, which may be attributed to the high evaporation rate of the water.

2.4. Characterization of HNTs. The zeta potential of dilute HNTs aqueous suspension was measured using a Zetasizer Nano ZS (Malvern Ltd., UK). The dilute HNTs aqueous suspension was dipped and dried on the carbon-film supported Cu-grid or a fresh mica sheet. The morphology of HNTs was observed using a Philips Tecnai 10 transmission electron microscope (TEM) under an accelerating voltage of 100 kV and using a NanoScope IIIa controller (Veeco Instruments Inc.) in tapping mode under ambient conditions. The hydrodynamic diameter and the size distribution of HNTs suspension (0.05 and 2 wt %) were detected by a Nano-ZS instrument (Malvern Instrument Ltd., UK). The hydrodynamic diameter was analyzed using cumulants.

2.5. Characterization of HNTs Concentric Ring Patterns. The optical micrographs and polarized optical microscopy (POM) micrographs of the patterned surfaces were examined using a ZEISS SteREO Discovery.V20, Germany instrument. The scanning electron microscopy (SEM) images of the patterned surfaces were obtained using a Zeiss Ultra 55 SEM machine at 5 kV. Before SEM observation, a layer of gold was sputtered. Atomic force microscopy (AFM) images were obtained using a NanoScope IIIa controller (Veeco Instruments Inc.) in tapping mode under ambient conditions.

2.6. Cell Culture on the Patterned HNTs Surfaces. C2C12 cells were purchased from the laboratory animal center of Sun Yat-Sen University, China. The cells were maintained in Dulbecco's modified Eagle's medium (DMEM, Life Technologies) supplemented with 10% fetal bovine serum (FBS, Life Technologies) and 1% penicillin (100 U/mL)/streptomycin (100 μg/mL). The cell lines were kept at 37 °C in a humidified atmosphere of 5% CO_2 in air as a monolayer culture in plastic culture plates (25 cm^2, Corning, NY, 14831). The cells were grown to ∼80% confluence before passaging with trypsin/ethylenediaminetetraacetic acid (EDTA) (Life Technologies) incubation for 2−3 min.

The HNTs ringlike pattern surfaces were first treated with APTES and then sterilized using microwave radiation in a commercial microwave oven at 700 W (2450 MHz) for 2 min. Then, HNTs surfaces were washed with 37 °C phosphate-buffered saline (PBS) solution twice. Afterward, the cell suspensions (2 mL, 1 × 10^4 cells/mL) were carefully added onto the surfaces. After 3 days, the cells were fixed using paraformaldehyde solution (4 wt % in PBS), permeabilized using Triton-X100 (0.2 wt % in PBS), and incubated with 1 mg/mL phalloidin-TRITC (Sigma) for 1 h at room temperature to label filamentous actin. After thoroughly being rinsed, the nuclei were stained with 5 mg/mL 4′,6-diamidino-2-phenylindole (DAPI, Sigma)

DOI: 10.1021/acs.langmuir.6b04460
Langmuir 2017, 33, 3088−3098

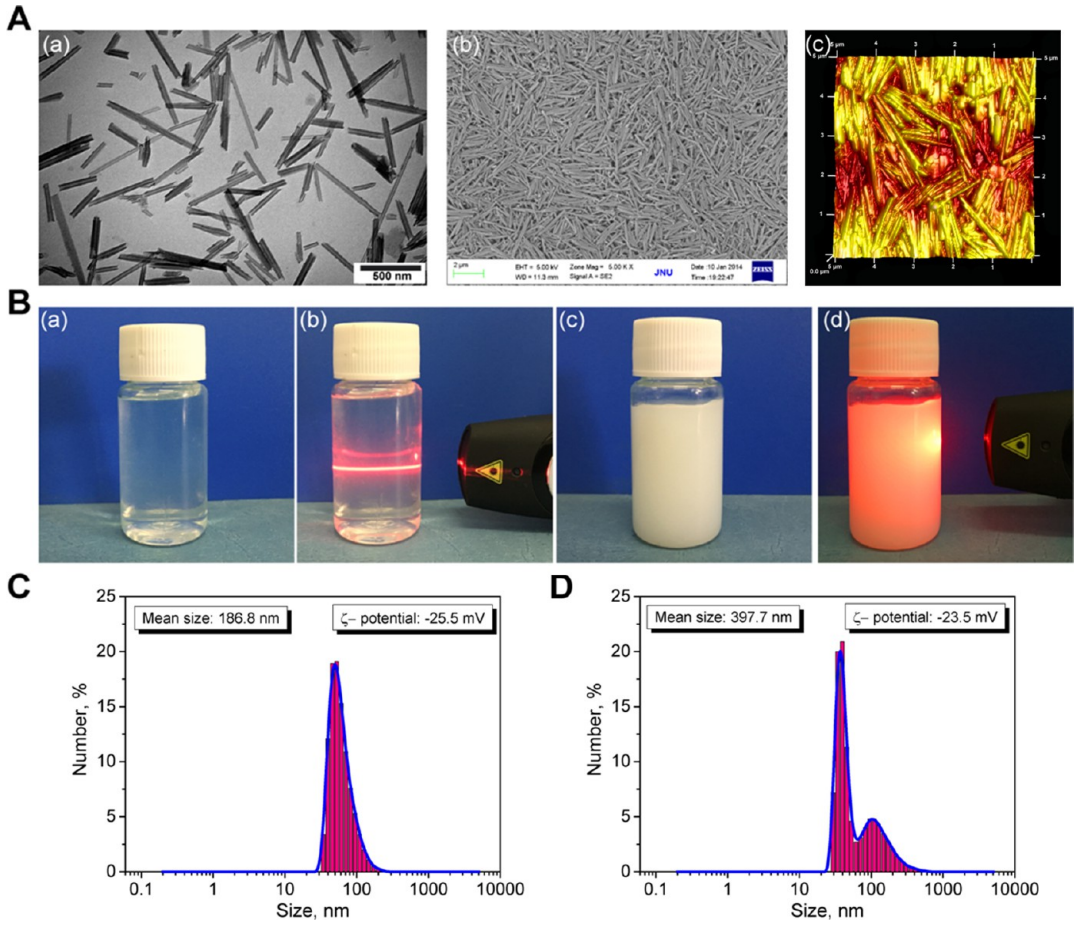

Figure 1. (A) Morphology of HNTs (a) TEM; (b) SEM; and (c) AFM; (B) HNTs aqueous suspension with different concentrations and the Tyndall effect of the suspension (a) 0.005%; (b) Tyndall effect; (c) 2%; and (d) no Tyndall effect; (C) DLS particle size distribution of 0.005% HNTs aqueous suspension; and (D) DLS particle size distribution of 2% HNTs aqueous suspension.

for 15 min. All stained samples were extensively rinsed with PBS before observation under an immunofluorescence microscope (XDY-2, Guangzhou Yuexian optical instrument Co., Ltd., China) mounted with a charge-coupled device (CCD).

3. RESULTS AND DISCUSSION

3.1. Characterization of HNTs. HNTs are ideal candidates for self-assembly studies because of their tubular morphology with a high aspect ratio, high dispersion ability in water without chemical modification, and low cost. Raw HNTs always contain impurities such as quartz and kaolinite, which lead to an inferior dispersion ability in water and nonuniform physical−chemical properties.[35] We purified the raw HNTs using a simple centrifugal process. The HNTs in the supernatant after 5000 rpm for 30 min were collected and considered to be high purity, as the impurities in the HNTs can sink to the bottom during the centrifugal process. Figure 1A shows the morphology of the purified HNTs. It can be seen that the HNTs show a typical empty tubular structure with a high dispersion ability, although the length of the tubes are different. Nearly no HNTs aggregate is found in the TEM image, which is essential for the self-assembly. The inner diameter, the outer diameter, and the length of HNTs are in the range of 12−20, 30−65, and 70−1200 nm, respectively. Also, it is found that the HNTs show an open end without any impurity on the inner or outer surface of the tubes. SEM and AFM results also confirm the morphology of the HNTs. The calculated aspect ratio of the HNTs are in the range of 2.3−42.4.

Figure 1B shows the appearance of HNTs suspension with different concentrations and the corresponding Tyndall effect photos. It is obvious that HNTs dilute suspension with 0.05 wt % concentration is completely transparent and homogeneous without any sedimentation. One can see a bluish discoloration of the suspension, which suggests the Tyndall effect by nanoparticles in a very fine suspension. When the light beam of a laser pointer is passed through the suspension, the nanotubes in water scatter the light in all directions, making it readily seen. This further confirms the nanoscale dispersion state of the nanotubes in water. However, when the suspension concentration of HNTs is 2 wt %, the appearance of the suspension turns opaque. The light beams cannot totally pass through the suspension, suggesting that part of the HNTs may aggregate into a large dimension. Figure 1C,D shows the particle size distribution of the two suspensions determined using dynamic light scattering (DLS). The dilute HNTs suspension (0.05 wt %) shows a very narrow size distribution with an average diameter of 186.8 ± 8.3 nm. The suspension with a high concentration shows two peaks around 37 and 103 nm in the size distribution curve. The average DLS diameter is determined to be 397.7 ± 20.4 nm. HNTs in the dilute HNTs suspension (0.05 wt %) present a faster dynamic behavior compared to the suspension with a high concentration, which suggests the enhancement of the repulsive interactions between

DOI: 10.1021/acs.langmuir.6b04460
Langmuir 2017, 33, 3088−3098

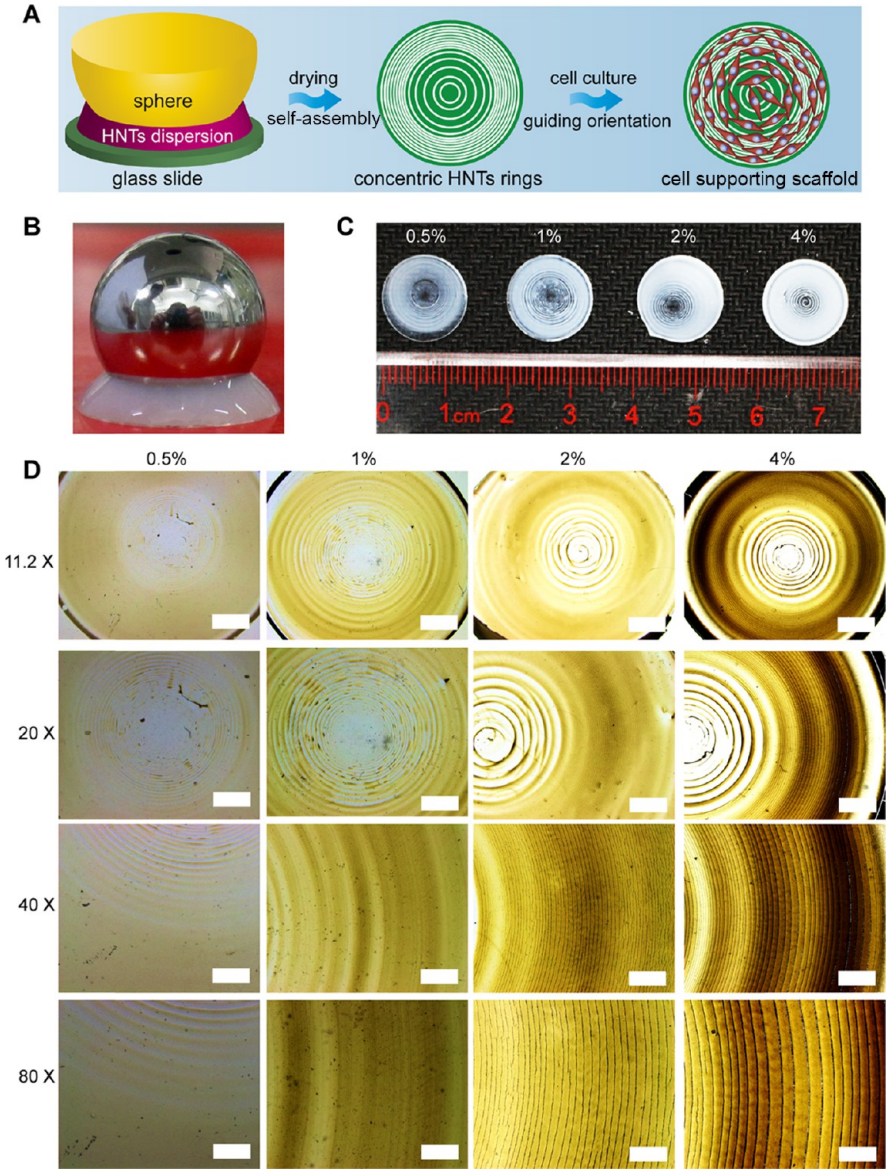

Figure 2. (A) Formation of concentric rings on the round glass slide via controlled evaporation of HNTs suspension in a sphere-flat confined space, (B) device photo of the sphere-flat confined space, (C) appearance of the formed concentric rings on the glass substrate, and (D) optical images illustrating the center part of the concentric rings pattern of the HNTs from different HNTs aqueous suspensions. The scale bar in (D) from top to bottom is 4000, 2000, 1000, and 500 μm.

the nanoparticles. In other words, the relatively large hydrodynamic diameter (R_h) value for HNTs in a high suspension concentration indicates the aggregation of nanotubes in this suspension.

As is known, DLS data is typically interpreted in terms of a spherelike particle. Therefore, the DLS results correspond to the diameter of a sphere that moves in the same way as the analyte particle. However, HNTs show a tubular-like morphology with a high aspect ratio. Thus, the DLS results do not truly correspond to a single dimension (length or diameter) of the nanotube, but rather to a combined value. Because DLS is a powerful technique for characterizing the size of HNTs due to its rapid analysis speed, it is convenient to estimate the diffusion coefficient (D_t) of HNTs. Here is a relation of D_t with the nanotube length (L) and diameter (d) from the analysis of carbon nanotubes reported by Nair et al.[40]

$$D_t = \frac{kT}{3\pi\eta L}[\ln(L/d) + 0.32]$$

where k is the Boltzmann constant, T is the thermodynamic temperature, η is the viscosity, L is the cylinder length, and d is the cylinder diameter.

The Stokes–Einstein relationship used to determine the particle size from the translational diffusion coefficient determined using DLS is given below.

$$D_t = \frac{kT}{3\pi\eta R_h}$$

where R_h is the hydrodynamic diameter which is the value obtained using DLS. Comparing the two equations, the tube length (L) and the tube diameter (d) can be given by the following equation.

DOI: 10.1021/acs.langmuir.6b04460
Langmuir 2017, 33, 3088−3098

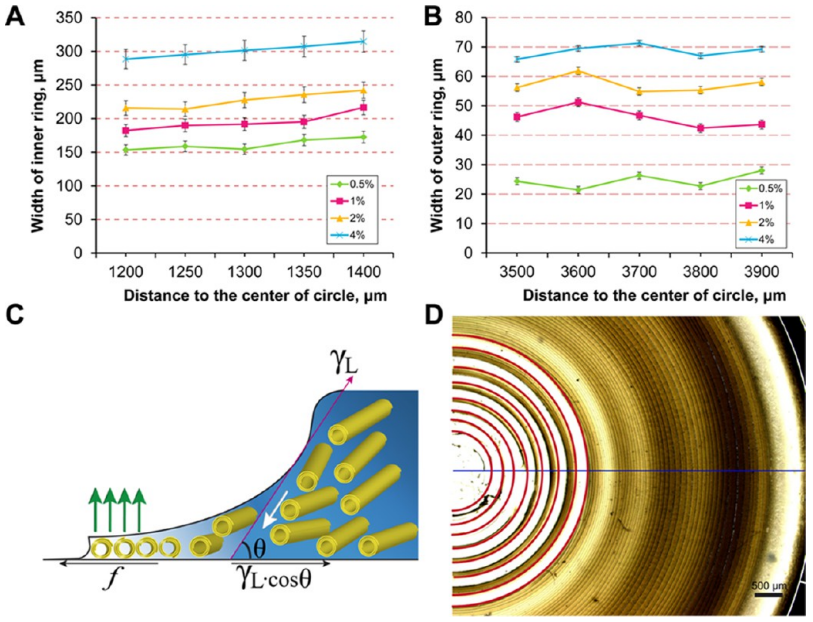

Figure 3. (A) Relationship between the width of the inner ring and the distance to the center of the circle; (B) relationship between the width of the outer ring and the distance to the center of the circle. *X* is the distance away from the contact center of the sphere and the glass sheet. (C) Schematic illustration of the thin meniscus formed at the three-phase contact line and the force balance. The arrow on the left represents the direction of the frictional force *f* generated by the deposition of particles at the contact line. The white arrow represents the moving direction of the HNTs caused by the convective force. The upward and right arrows represent γ_L and $\gamma_L \cos\theta$, respectively, with θ being the contact angle between the suspensions and the substrate. (D) Optical image of the concentric ring pattern formed from 4 wt % HNTs suspension with illustration of the inner ring width determination method.

$$R_h = \frac{L}{\ln(L/d) + 0.32}$$

Using the L and d values for the used HNTs from the TEM result (d = 30−65 nm, L = 70−1200 nm), the calculated R_h is in the range from 60 to 370 nm, depending on the chosen value for length and diameter. This range fits well with the determined DLS R_h data above; if we use the most common dimension value of HNTs as d = 50 nm and L = 500 nm, then the calculated R_h is 190.8 nm. This value is very close to the determined DLS diameter (186.8 ± 8.3 nm) for dilute HNTs suspension (0.05 wt %). Moreover, if the length of the nanotube is unknown, it can be calculated with the same equation using the measured R_h from the DLS (assume 187 nm based on the DLS range) and a diameter of approximately 50 nm. The length of the HNTs are calculated with a value of 485 nm. Thus, the present DLS measurement results are consistent with the theoretical calculation according to Nair's equation.

The surface potentials of the nanoparticles have a significant effect on the colloidal stability for the self-assembly behavior. Zeta potentials of the 0.05 and 2 wt % suspensions are −25.5 and −23.5 mV, respectively. The repulsive interactions between the nanoparticles gradually decrease when increasing the concentration of the suspension, which leads to a slightly decreased surface potentials. The used HNTs suspension for self-assembly was obtained by concentrating a super stable dilute suspension obtained from the supernatant after centrifugation of 5% HNTs suspension. From the macroscopic observation and TEM determination, it can be seen that the HNTs suspension is stable in the assembly process. In total, the features of HNTs, that is, the unique tubular structure with a high aspect ratio and a good dispersion ability in water with high stability, make them good candidates for self-assembly into hierarchical architectures.

3.2. Formation of HNTs Concentric Rings in a Sphere-Flat Confined Space. A sphere-on-flat geometry as a confined space has been widely used to study the evaporation-induced assembly process of polymers or nanoparticles.[36−39] Both the glass sphere (or stainless steel sphere) and the round glass sheet were firmly fixed at the top and the bottom in a sample holder. After they contacted, 200 μL of HNTs aqueous suspension was loaded via a pipette and trapped between the sphere and the glass sheet because of the capillary force, so that a capillary-held HNTs suspension formed with an evaporation rate highest at the capillary edge (Figure 2A). This results in a controlled and repetitive "stick-slip" motion of the three-phase contact line that moves toward the contact center of the sphere/glass sheet during the course of water evaporation. As a consequence, gradient concentric rings consisting of HNTs were formed on the glass substrate. Also, regular rings pattern can also be formed on the suspension contact surface of a stainless steel sphere (Figure S1). The regular rings of HNTs can be used as a cell culture scaffold and will guide the oriented growth of cells. The appearance of the drying device and the formed ring pattern are shown in Figure 2B,C, respectively. It can be seen that the HNTs coating on the glass substrate shows different thicknesses and morphologies. With the increase in the suspension concentration, the thickness of the HNTs coating increases and the ring structure is much clearer with the naked eye. Although all coatings exhibit translucence, the light transmission is sufficient for observing the cell morphology via immunofluorescent staining.

Figure 2D shows the optical micrograph of the HNTs ring pattern formed from different suspensions. It can be seen that regular rings with the same center but with different diameters were formed on the glass substrate. This result can be attributed to the solvent evaporation-induced self-assembly of HNTs in the confined space. Similar to the coffee ring effect,

DOI: 10.1021/acs.langmuir.6b04460
Langmuir 2017, 33, 3088−3098

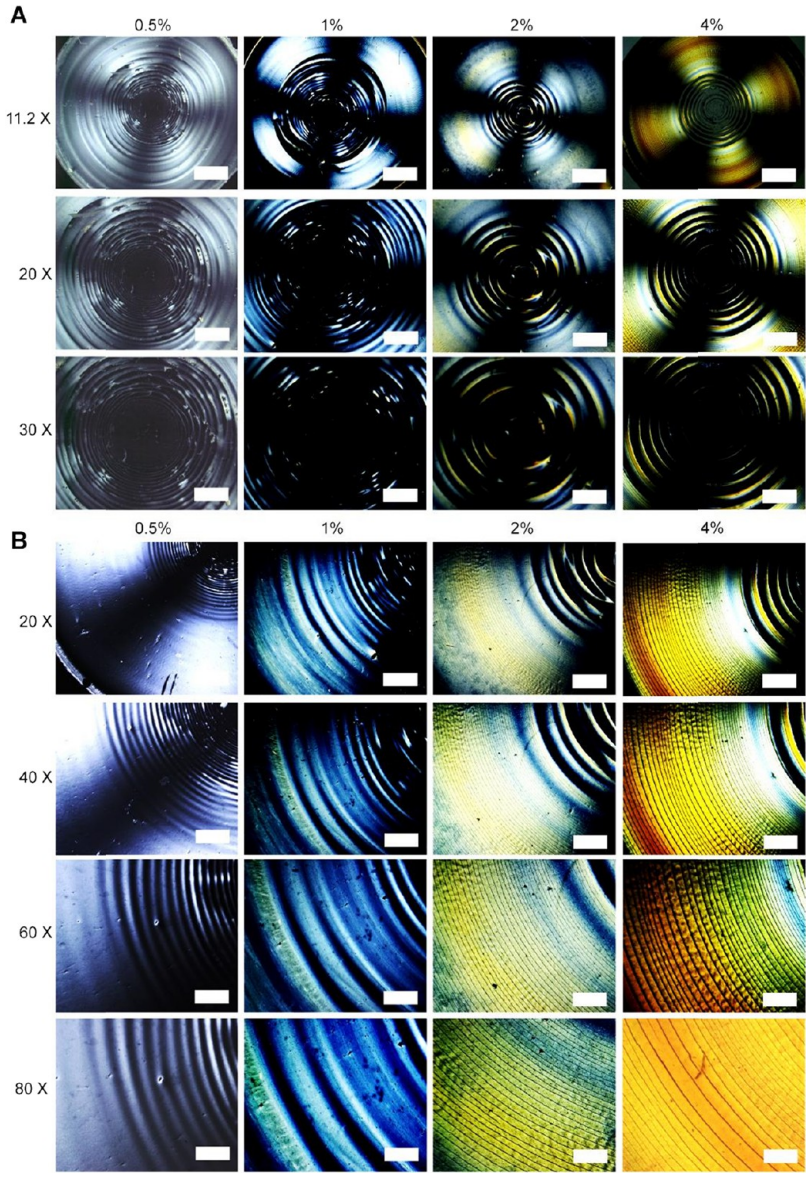

Figure 4. (A) POM photos illustrating the center part of the HNTs concentric rings pattern from different HNTs concentrations; (B) POM photos illustrating the quarter of the HNTs concentric rings pattern from different HNTs concentrations. The scale bar for 11.2×, 20×, 30×, 40×, 60×, and 80× is 4000, 2000, 1333, 1000, 667, and 500 μm, respectively.

the loss of water at the capillary edges causes the pinning of the solid−liquid−gas three phase contact line (i.e., "stick"), thereby forming the outermost ring. Upon drying, the contact angle of the capillary edge decreases gradually to a critical angle at which the capillary force (depinning force) becomes larger than the pinning force.[37] This leads to a hop of the contact line to a new position (i.e., "slip"), where a new ring deposits and gradually forms. The repetitive of the "stick−slip" motion of the contact line gives rise to the formation of concentric rings of HNTs toward the contact center of the sphere-on-flat geometry.

The suspension concentration has a significant impact on the formed ring pattern structure. A relatively uniform HNTs coating with a small thickness is found after the evaporation of 0.5 wt % HNTs suspension. Only raised and nonindependent rings are found in the inner region of the coating. In the outer region of the coating, no regular ring can be identified from the images. This is because the depinning force (i.e., capillary force) is not strong enough to cause the three-phase contact line to jump to a new position inward during the drying of the 0.5 wt % HNTs suspension. The depinning force cannot completely overcome the pinning force exerted by the deposition of HNTs. Thus, a continuous HNTs film with some crack (will be shown in the following SEM result) is formed in the outer region. With the increase in the suspension concentration, the thickness of the HNTs coating becomes thicker and thicker. Also, the formed ring is more regular and distinct as observed from the series of images. It should also be noted that the ring dimension is different in the inner and outer regions of the glass sheet. The height of the rings in the outer region is larger than that in the inner. This is especially obvious in the ring structure formed from the 4 wt % HNTs suspension. From the outer region to the inner region, the ring patterns turn from black to semitransparent, suggesting the decrease in the height of the ring strips.

The concentrations of HNTs will determine the number of particles supplied to the growing ring region, which is directly

DOI: 10.1021/acs.langmuir.6b04460
Langmuir 2017, 33, 3088−3098

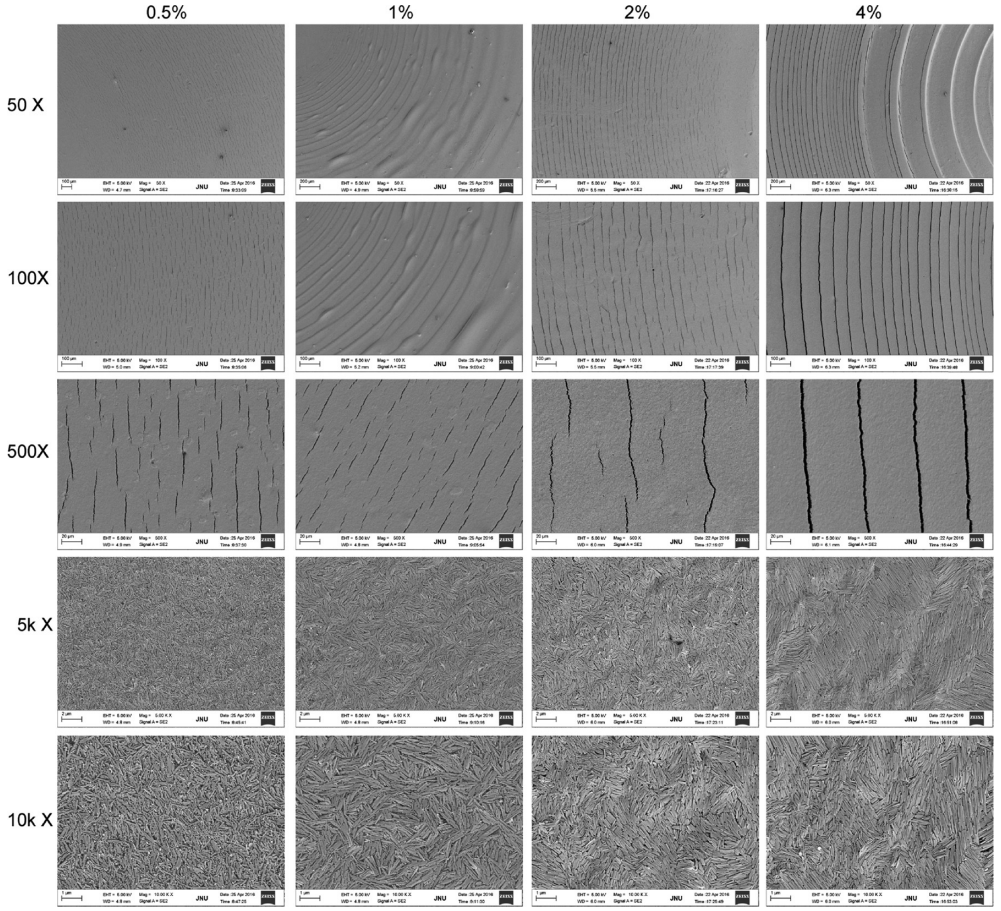

Figure 5. SEM photos of the concentric rings pattern of the HNTs formed from different HNTs suspensions.

related to the width and thickness of the ring strips. The widths of the ring strips in the inner and outer regions are compared in Figure 3A,B. The width of the ring, both in the inner and outer regions, is found to increase with increasing the suspension concentration. For example, the width of the ring strips in the outer region formed from the 4 wt % HNTs suspension is 65.8−71.3 μm, whereas it is 21.5−28.0 μm for that formed from the 0.5 wt % suspension. This can be understood by the different force balance during the drying process (Figure 3C). The surface roughness is generated by the deposition of HNTs to produce a frictional force f (pinning force). As the evaporation proceeds, the initial contact angle (θ) of the capillary edge decreases gradually to a critical angle, at which the capillary force (depinning force, $\gamma_L \cos \theta$) becomes larger than the pinning force f.[41] The capillary force pulls the liquid inward, which leads to the jumping of the contact line to a new position and the formation of a new ring. At higher HNTs concentrations, part of the tubes form bundles or aggregates. When these nanotube bundles deposit at the contact line, the ring strip is thick and the corresponding generated frictional force f increases, which is larger than the capillary force $\gamma_L \cos \theta$. The pinning time is long for the suspension with a high concentration; as a result, the width of the rings increases compared with the relatively low suspension concentration. The result is in agreement with the previously reported influence of suspension concentrations on the width of the strips.[42]

It should also be noted that there is a transition from dense concentric ring structure with a small space to sparse concentric ring structure with a relatively large space at around 2400 μm distance to the sphere/glass sheet contact center (Figure 3D). This can be understood by the following fact. At the late stage of drying, the suspension front is very close to the contact center of the sphere and the glass sheet, which leads to the decreased contact angle (θ) of the meniscus because of the decrease in curvature. This consequently results in the increase in the depinning force ($\gamma_L \cos \theta$). The pinning force f remains unchanged, so the three-phase contact line can jump a much farther distance to a new position. At the point very near the contact center of the sphere and the glass sheet, no regular pattern can be formed, which is due to the instability raised by the very slow evaporation rate of water.[36] In summary, the simple sphere-on-flat geometry can provide a confined environment to control the HNTs suspension evaporation, which in turn regulates the regular ring pattern formation with excellent reproducibility. The methods described herein can be readily extended to the fabrication of gradient concentric ring pattern of other type nanoparticles (e.g., cellulose nanocrystal) for biomedical applications with little toxicity.

3.3. Cholesteric Structure and Microstructure of the Formed HNTs Concentric Rings Pattern. When the formed pattern was imaged under crossed polarizers, a pronounced Maltese crosslike pattern was observed even in the ring pattern formed from the 0.5 wt % HNTs suspension (Figure 4A). The cross is a white eight-pointed cross having the form of four "V"-shaped elements, each joining the others at its vertex, leaving the other two tips spread outward symmetrically. This is caused by the radial ordering of the HNTs within the ring during the

DOI: 10.1021/acs.langmuir.6b04460
Langmuir 2017, 33, 3088−3098

drying process. The superimposed Maltese cross pattern is due to the isoclines of the radial cholesteric helix axis aligned with the axes of the crossed polarizers, in agreement with a planar anchoring of the local director of HNTs with the droplet interface.[2] When increasing the concentration of the HNTs suspension, the POM images gradually transfer from nearly black and white to being colorful. This suggests that both hierarchical cholesteric architectures and thickness of the HNTs coating increase with the increase in the concentration of the HNTs suspension. The formed HNTs concentric rings are just like polymer spherulites with a similar refraction phenomenon under polarized light. Consistent with the optical micrograph above, the POM images also demonstrate that the width of the ring strips increases with the increase in the concentration of the HNTs suspension. All of the formed HNTs ring patterns are symmetrical; the Maltese cross patterns with intervals of bright and dark regions can rotate when one rotates the HNTs coating (Movie S1).

The microstructure and the nanotube alignment of the ring strips were further investigated using SEM (Figure 5). Consistent with the results from the optical images and POM images, all of the HNTs coating shows highly regular and concentric ring structures. The ring width depends both on the location in the coating and the suspension concentration. The ring is dense in the outer region and sparse in the inner region for all samples. For the coating formed from low concentration HNTs suspensions (0.5 and 1 wt %), the concentric rings are linked by shallow and discontinuous cracks, whereas in the coating formed from relatively high concentration HNTs suspensions (2 and 4 wt %), deep and continuous cracks are formed. The strip width and crack widths (spacing between the adjacent rings) increase with the concentration of the HNTs suspension. For example, the width of the cracks is ~1.66 μm in the ring pattern formed from the 0.5 wt % HNTs suspension, whereas it is ~2.55 μm in the ring pattern formed from the 4 wt % HNTs suspension.

From the high-magnification images of the coating from different HNTs suspensions, it can be seen that the tubes alignment is largely different from that of a random distributed HNTs coating. A topological defect in the orientation of rodlike substance with a high aspect ratio, referred to as disclination, has been identified for all samples, especially at high HNTs concentrations. The formed disclination pattern further indicates the transition from isotropic to a liquid-crystal phase during the water evaporation process of the suspensions.[11] The nanotubes can be aligned to form the disclination pattern because of the minimum energy, which is related to Frank elastic continuum theory.[43] According to Frank elastic continuum theory, the disclinations represented arrangements of minimum energy that can be distinguished by their strength (s), which corresponds to the number of rotations (in multiples of 2π) over a path encircling the disclination and constant parameter (c), which relates the axial position in the plane around the disclination core (polar angle θ), and the director orientation angle φ.[44] The equation $\varphi(\theta) = s\theta + c$ can be used for characterization of the disclinations in an ordered structure such as a liquid crystal. There are two types of disclinations with half integer strength ($s = +1/2$, corresponding to the parabolic disclination; $s = -1/2$, corresponding to the hyperbolic disclination) and 1 integer strength ($s = -1$, corresponding to the hyperbolic with four-fold symmetry; $s = +1$, corresponding to radial, circular, or spiral)[11](Figure 6A). Because the energy related to the disclinations depends on s^2,

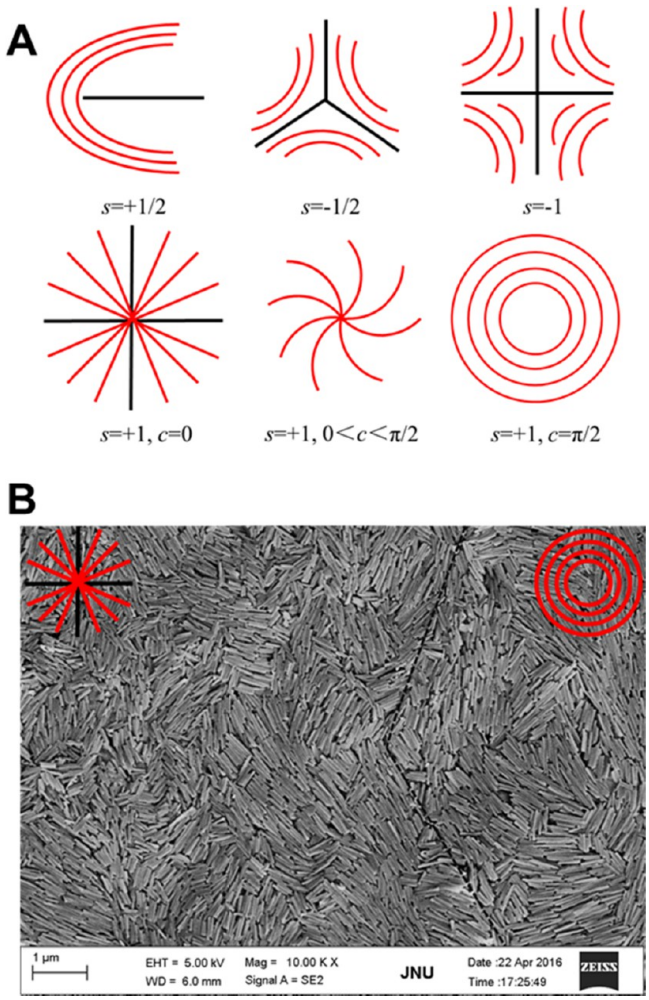

Figure 6. (A) Frank continuum theory prediction of topological defects associated with disclinations of $s = \pm 1/2$ and ± 1; (B) SEM image of HNTs disclination patterns from 2% HNTs aqueous suspension.

the half integer strength disclinations ($s = \pm 1/2$) are topologically more stable than the integer defects ($s = \pm 1$). Figure 6B shows the SEM image of the HNTs disclination pattern from the 2% HNTs suspension. The HNTs disclination patterns exhibit a radial shape in the left part of the image, while exhibiting a circular shape in the right part of the image. All of the radial and circular shapes are assigned to $s = +1$, suggesting the formation a less stable topological defect during the evaporation of HNTs suspension under the sphere-on-flat confinements. A previous study also revealed a similar disclination pattern of HNTs, which was attributed to the presence of impurities or short tubes in the HNTs samples.[11] After carefully checking the formed HNTs patterns from different suspensions, it can be found that most of them exhibit $s = +1$ disclination with a radial or circular alignment. However, the pattern formed from the 0.5% HNTs suspension does not belong to any disclination type, which is attributed to the fact that a very dilute suspension cannot generate an ordered nanotube alignment. The AFM results also confirm the SEM result on the alignment of the HNTs in the coating (Figure S2). The regularly oriented HNTs ring pattern can be used to tailor the growth and alignment behavior of cells for tissue engineering scaffolds or as a model for nanofabrication.

DOI: 10.1021/acs.langmuir.6b04460
Langmuir 2017, 33, 3088−3098

3.4. Cell Orientation on the Concentric Rings Pattern of HNTs. The differentiation and alignment of cells play an essential role in the formation and repair of tissues. Cells can attach to artificial surfaces via focal adhesions, connecting the surface to the cytoskeleton. The interactions between the cell and the substrates are mainly dominated by surface chemistry (including the presence of ligands), electrostatic charge, wettability, and elastic modulus.[45] Micro- and nanosized topographical surfaces can guide alignment, migration of cells, or outgrowth of neurites along a specific orientation.[6,8] To probe the ability of cells to respond to surface topography, many patterned substrata, such as grooved surfaces, are commonly used. The patterned surfaces always lead to physical guidance of the direction and reorganization of the cytoskeleton. C2C12 myoblasts have commonly served as a model to study the guided alignment behavior of cells. Figure 7

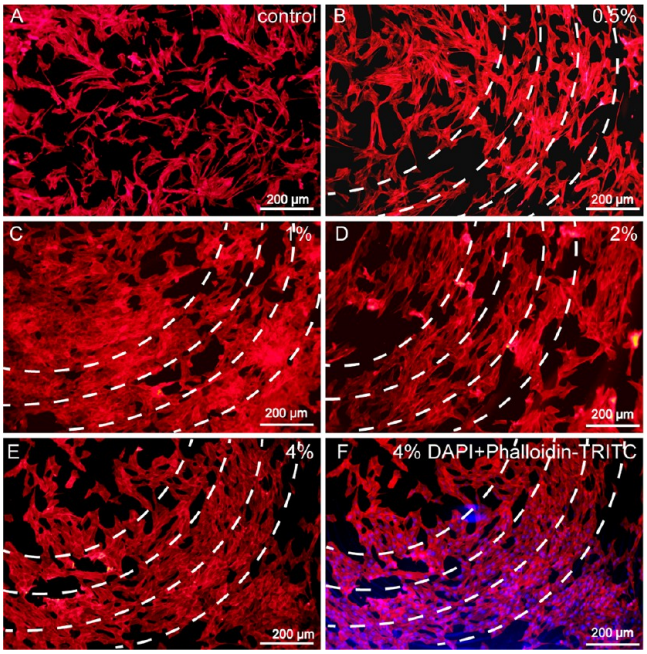

Figure 7. Immunofluorescence staining of F-actin (red, TRITC) for C2C12 cells grown on the HNTs concentric rings pattern from different HNTs concentrations: (A) control; (B) 0.5 wt % HNTs; (C) 1 wt % HNTs; (D) 2 wt % HNTs; (E) 4 wt % HNTs; and (F) 4 wt % HNTs (with DAPI (nucleus, blue) and phalloidin-TRITC double staining). The white dotted line in (B–F) illustrates the alignment direction of the cells on HNTs ring pattern.

shows the fluorescence images of C2C12 cells growing on the prepared HNTs ring pattern surfaces. The cells can spread out on the substrates for all groups, and no dead cells can be detected, indicating the good cytocompatibility of the HNTs pattern. In contrast to the C2C12 cells cultured on a smooth glass surface (Figure 7A), C2C12 cells cultured on the concentric ring pattern of HNTs can align perpendicular to the ring direction (Figure 7B–F). In a smooth glass surface without HNTs ring patterns, C2C12 cells display rhomboid shape and are randomly distributed without a preferred orientation phenomenon. However, C2C12 cells cultured on the concentric ring surface of HNTs tend to be spindle-shaped and grow along the ring direction. Because the cracks between the adjacent rings are narrow (~2 μm), the cells cannot grow in the cracks because of the relatively large dimension of the cells. The cell can be fixed and aligned on the HNTs rings because of the strong interactions between the nanotopology of HNTs and the cell pseudopods. The phenomenon is just like how the players run around a playground racetrack. The cells are like the players, whereas the HNTs ring is like the track. It is also clear that in the inner part of the ring pattern surface (such as the upper left corner in Figure 7B,E) the cells are randomly distributed because of the absence of the regular ring pattern as illustrated above. The present results on HNTs pattern for the regulation of C2C12 cell behavior are significant because the HNTs have high cytocompatibility and can be used as biomaterials for many applications as showed in the previous studies.[16−18,21,46]

4. CONCLUSIONS

HNTs have a tubular structure with a high aspect ratio and exhibit a high water dispersion ability, which make them a good model for studying the self-assembly behavior of nanoparticles. Concentric ring patterns consisting of HNTs with hierarchical cholesteric architectures can be prepared by an evaporation-induced self-assembly process in a sphere-on-flat geometry. The widths of the inner and outer rings and the spacing between the adjacent rings increase with an increase in the concentration of the HNTs suspension. The HNTs ring patterns show a pronounced Maltese cross-like phenomenon under crossed polarizers, which suggests the formation of hierarchical cholesteric architectures. A disclination alignment of HNTs with strength of $s = +1$ is found in the ring strips, especially with a high concentration of the HNTs suspension. The patterned HNTs rough surfaces show low cytotoxicity and are used as cell supporting scaffold. The HNTs rings can direct the orientation of the C2C12 myoblasts cells perpendicular to the rings. This work provides a simple, repeatable, mild, and high-efficiency method for obtaining HNTs hierarchical architectures that offers a large variety of applications, for example, in vascular grafts and skin regeneration.

■ ASSOCIATED CONTENT

Supporting Information

The Supporting Information is available free of charge on the ACS Publications website at DOI: 10.1021/acs.langmuir.6b04460.

Maltese cross pattern rotating when one rotates the HNTs ring pattern (AVI)

Photograph of a stainless steel sphere showing the regular rings pattern formed on the contact surface with the HNTs suspension and AFM images of the HNTs concentric ring pattern from different HNTs concentrations (PDF)

■ AUTHOR INFORMATION

Corresponding Authors

*E-mail: liumx@jnu.edu.cn. Phone: (86)20-85226663. Fax: (86)20-85223271 (M.L.).

*E-mail: tcrz9@jnu.edu.cn (C.Z.).

ORCID

Mingxian Liu: 0000-0002-5466-3024

Notes

The authors declare no competing financial interest.

DOI: 10.1021/acs.langmuir.6b04460
Langmuir 2017, 33, 3088−3098

■ ACKNOWLEDGMENTS

This work was financially supported by the National High Technology Research and Development Program of China (2015AA020915), the National Natural Science Foundation of China (51473069 and 51502113), and the Guangdong Natural Science Funds for Distinguished Young Scholar (S2013050014606), the Science and Technology Planning Project of Guangdong Province (2014A020217006), the Guangdong Special Support Program (2014TQ01C127), the Special Fund for Ocean-Scientific Research in the Public Interest (201405105), and the Pearl River S&T Nova Program of Guangzhou (201610010026).

■ REFERENCES

(1) Tang, Z.; Kotov, N. A.; Magonov, S.; Ozturk, B. Nanostructured Artificial Nacre. *Nat. Mater.* **2003**, *2*, 413−418.
(2) Parker, R. M.; Frka-Petesic, B.; Guidetti, G.; Kamita, G.; Consani, G.; Abell, C.; Vignolini, S. Hierarchical Self-Assembly of Cellulose Nanocrystals in a Confined Geometry. *ACS Nano* **2016**, *10*, 8443−8449.
(3) Davidson, P.; Gabriel, J.-C. P. Mineral Liquid Crystals. *Curr. Opin. Colloid Interface Sci.* **2005**, *9*, 377−383.
(4) Michot, L. J.; Bihannic, I.; Maddi, S.; Funari, S. S.; Baravian, C.; Levitz, P.; Davidson, P. Liquid−Crystalline Aqueous Clay Suspensions. *Proc. Natl. Acad. Sci. U.S.A.* **2006**, *103*, 16101−16104.
(5) Xu, Z.; Gao, C. Aqueous Liquid Crystals of Graphene Oxide. *ACS Nano* **2011**, *5*, 2908−2915.
(6) Lin, Y.; Balizan, E.; Lee, L. A.; Niu, Z.; Wang, Q. Self-Assembly of Rodlike Bio-Nanoparticles in Capillary Tubes. *Angew. Chem., Int. Ed.* **2009**, *49*, 868−872.
(7) Li, T.; Winans, R. E.; Lee, B. Superlattice of Rodlike Virus Particles Formed in Aqueous Solution through Like-Charge Attraction. *Langmuir* **2011**, *27*, 10929−10937.
(8) Zan, X.; Feng, S.; Balizan, E.; Lin, Y.; Wang, Q. Facile Method for Large Scale Alignment of One Dimensional Nanoparticles and Control over Myoblast Orientation and Differentiation. *ACS Nano* **2013**, *7*, 8385−8396.
(9) Flauraud, V.; Mastrangeli, M.; Bernasconi, G. D.; Butet, J.; Alexander, D. T. L.; Shahrabi, E.; Martin, O. J. F.; Brugger, J. Nanoscale Topographical Control of Capillary Assembly of Nanoparticles. *Nat. Nanotechnol.* **2016**, DOI: 10.1038/nnano.2016.179.
(10) Liu, M.; He, R.; Yang, J.; Zhao, W.; Zhou, C. Stripe-Like Clay Nanotubes Patterns in Glass Capillary Tubes for Capture of Tumor Cells. *ACS Appl. Mater. Interfaces* **2016**, *8*, 7709−7719.
(11) Zhao, Y.; Cavallaro, G.; Lvov, Y. Orientation of Charged Clay Nanotubes in Evaporating Droplet Meniscus. *J. Colloid and Interface Sci.* **2015**, *440*, 68−77.
(12) Collet, M.; Salomon, S.; Klein, N. Y.; Seichepine, F.; Vieu, C.; Nicu, L.; Larrieu, G. Large-Scale Assembly of Single Nanowires through Capillary-Assisted Dielectrophoresis. *Adv. Mater.* **2015**, *27*, 1268−1273.
(13) Xu, Z.; Gao, C. Graphene Chiral Liquid Crystals and Macroscopic Assembled Fibres. *Nat. Commun.* **2011**, *2*, 571.
(14) Lin, Y.; Su, Z.; Balizan, E.; Niu, Z.; Wang, Q. Controlled Assembly of Protein in Glass Capillary. *Langmuir* **2010**, *26*, 12803−12809.
(15) Han, W.; Lin, Z. Learning from "Coffee Rings": Ordered Structures Enabled by Controlled Evaporative Self-Assembly. *Angew. Chem., Int. Ed.* **2012**, *51*, 1534−1546.
(16) Lvov, Y.; Wang, W.; Zhang, L.; Fakhrullin, R. Halloysite Clay Nanotubes for Loading and Sustained Release of Functional Compounds. *Adv. Mater.* **2016**, *28*, 1227−1250.
(17) Mitchell, M. J.; Chen, C. S.; Ponmudi, V.; Hughes, A. D.; King, M. R. E-Selectin Liposomal and Nanotube-Targeted Delivery of Doxorubicin to Circulating Tumor Cells. *J. Controlled Release* **2012**, *160*, 609−617.
(18) Liu, M.; Chang, Y.; Yang, J.; You, Y.; He, R.; Chen, T.; Zhou, C. Functionalized Halloysite Nanotube by Chitosan Grafting for Drug Delivery of Curcumin to Achieve Enhanced Anticancer Efficacy. *J. Mater. Chem. B* **2016**, *4*, 2253−2263.
(19) Liu, M.; Wu, C.; Jiao, Y.; Xiong, S.; Zhou, C. Chitosan−Halloysite Nanotubes Nanocomposite Scaffolds for Tissue Engineering. *J. Mater. Chem. B* **2013**, *1*, 2078−2089.
(20) Liu, M.; Jia, Z.; Jia, D.; Zhou, C. Recent Advance in Research on Halloysite Nanotubes-Polymer Nanocomposite. *Prog. Polym. Sci.* **2014**, *39*, 1498−1525.
(21) Lvov, Y.; Abdullayev, E. Functional Polymer−Clay Nanotube Composites with Sustained Release of Chemical Agents. *Prog. Polym. Sci.* **2013**, *38*, 1690−1719.
(22) Luo, Z.; Song, H.; Feng, X.; Run, M.; Cui, H.; Wu, L.; Gao, J.; Wang, Z. Liquid Crystalline Phase Behavior and Sol−Gel Transition in Aqueous Halloysite Nanotube Dispersions. *Langmuir* **2013**, *29*, 12358−12366.
(23) Zhao, N.; Liu, Y.; Zhao, X.; Song, H. Liquid Crystal Self-Assembly of Halloysite Nanotubes in Ionic Liquids: A Novel Soft Nanocomposite Ionogel Electrolyte with High Anisotropic Ionic Conductivity and Thermal Stability. *Nanoscale* **2016**, *8*, 1545−1554.
(24) Mohtashim, H. S.; Kurt, E. G. The First Biopolymer-Wrapped Non-Carbon Nanotubes. *Nanotechnology* **2008**, *19*, 075604.
(25) Cavallaro, G.; Lazzara, G.; Milioto, S.; Parisi, F.; Sanzillo, V. Modified Halloysite Nanotubes: Nanoarchitectures for Enhancing the Capture of Oils from Vapor and Liquid Phases. *ACS Appl. Mater. Interfaces* **2014**, *6*, 606−612.
(26) Cavallaro, G.; Lazzara, G.; Milioto, S. Exploiting the Colloidal Stability and Solubilization Ability of Clay Nanotubes/Ionic Surfactant Hybrid Nanomaterials. *J. Phys. Chem. C* **2012**, *116*, 21932−21938.
(27) Fakhrullina, G. I.; Akhatova, F. S.; Lvov, Y. M.; Fakhrullin, R. F. Toxicity of Halloysite Clay Nanotubes in Vivo: A *Caenorhabditis elegans* Study. *Environ. Sci.: Nano* **2015**, *2*, 54−59.
(28) Massaro, M.; Riela, S.; Meo, P. L.; Noto, R.; Cavallaro, G.; Milioto, S.; Lazzara, G. Functionalized Halloysite Multivalent Glycocluster as a New Drug Delivery System. *J. Mater. Chem. B* **2014**, *2*, 7732−7738.
(29) Yang, F.; Murugan, R.; Wang, S.; Ramakrishna, S. Electrospinning of Nano/Micro Scale Poly(L-Lactic Acid) Aligned Fibers and Their Potential in Neural Tissue Engineering. *Biomaterials* **2005**, *26*, 2603−2610.
(30) Zhang, Y.; Li, C.; Chan, V.; Kang, Y. Biomechanistic Study of Smooth Muscle Cell Sheet During Circumferential Alignment in Circular Micropatterns. *ACS Biomater. Sci. Eng.* **2015**, *1*, 549−558.
(31) Zhong, S.; Teo, W. E.; Zhu, X.; Beuerman, R. W.; Ramakrishna, S.; Yung, L. Y. L. An Aligned Nanofibrous Collagen Scaffold by Electrospinning and Its Effects on in Vitro Fibroblast Culture. *J. Biomed. Mater. Res., Part A* **2006**, *79*, 456−463.
(32) Dahlin, R. L.; Kasper, F. K.; Mikos, A. G. Polymeric Nanofibers in Tissue Engineering. *Tissue Eng., Part B* **2011**, *17*, 349−364.
(33) Sarkar, S.; Dadhania, M.; Rourke, P.; Desai, T. A.; Wong, J. Y. Vascular Tissue Engineering: Microtextured Scaffold Templates to Control Organization of Vascular Smooth Muscle Cells and Extracellular Matrix. *Acta Biomater.* **2005**, *1*, 93−100.
(34) Qin, D.; Xia, Y.; Whitesides, G. M. Soft Lithography for Micro- and Nanoscale Patterning. *Nat. Protoc.* **2010**, *5*, 491−502.
(35) Rong, R.; Xu, X.; Zhu, S.; Li, B.; Wang, X.; Tang, K. Facile Preparation of Homogeneous and Length Controllable Halloysite Nanotubes by Ultrasonic Scission and Uniform Viscosity Centrifugation. *Chem. Eng. J.* **2016**, *291*, 20−29.
(36) Xu, J.; Xia, J.; Lin, Z. Evaporation-Induced Self-Assembly of Nanoparticles from a Sphere-on-Flat Geometry. *Angew. Chem.* **2007**, *119*, 1892−1895.
(37) Hong, S. W.; Xu, J.; Lin, Z. Template-Assisted Formation of Gradient Concentric Gold Rings. *Nano Lett.* **2006**, *6*, 2949−2954.
(38) Xu, J.; Xia, J.; Hong, S. W.; Lin, Z.; Qiu, F.; Yang, Y. Self-Assembly of Gradient Concentric Rings via Solvent Evaporation from a Capillary Bridge. *Phys. Rev. Lett.* **2006**, *96*, 066104.

DOI: 10.1021/acs.langmuir.6b04460
Langmuir 2017, 33, 3088−3098

(39) Hong, S. W.; Xia, J.; Byun, M.; Zou, Q.; Lin, Z. Mesoscale Patterns Formed by Evaporation of a Polymer Solution in the Proximity of a Sphere on a Smooth Substrate: Molecular Weight and Curvature Effects. *Macromolecules* **2007**, *40*, 2831−2836.
(40) Nair, N.; Kim, W.-J.; Braatz, R. D.; Strano, M. S. Dynamics of Surfactant-Suspended Single-Walled Carbon Nanotubes in a Centrifugal Field. *Langmuir* **2008**, *24*, 1790−1795.
(41) Hong, S. W.; Jeong, W.; Ko, H.; Kessler, M. R.; Tsukruk, V. V.; Lin, Z. Directed Self-Assembly of Gradient Concentric Carbon Nanotube Rings. *Adv. Funct. Mater.* **2008**, *18*, 2114−2122.
(42) Lin, Y.; Su, Z.; Xiao, G.; Balizan, E.; Kaur, G.; Niu, Z.; Wang, Q. Self-Assembly of Virus Particles on Flat Surfaces via Controlled Evaporation. *Langmuir* **2011**, *27*, 1398−1402.
(43) Frank, F. C. Liquid Crystals. On the Theory of Liquid Crystals. *Discuss. Faraday Soc.* **1958**, *25*, 19−28.
(44) Zhang, S.; Terentjev, E. M.; Donald, A. M. Optical Microscopy Study for Director Patterns around Disclinations in Side-Chain Liquid Crystalline Polymer Films. *J. Phys. Chem. B* **2005**, *109*, 13195−13199.
(45) Peterbauer, T.; Yakunin, S.; Siegel, J.; Hering, S.; Fahrner, M.; Romanin, C.; Heitz, J. Dynamics of Spreading and Alignment of Cells Cultured in Vitro on a Grooved Polymer Surface. *J. Nanomater.* **2011**, *2011*, 413079.
(46) Liu, M.; Shen, Y.; Ao, P.; Dai, L.; Liu, Z.; Zhou, C. The Improvement of Hemostatic and Wound Healing Property of Chitosan by Halloysite Nanotubes. *RSC Adv.* **2014**, *4*, 23540−23553.

DOI: 10.1021/acs.langmuir.6b04460
Langmuir 2017, 33, 3088−3098